MIXED-MODE FRACTURE OF STEEL AND CERAMICS

A. R. Rosenfield*

Experimental techniques for generating combined opening/shear fracture-toughness envelopes are described, both for ceramics and steels. The ceramic envelopes are applied to the study of debris formation in sliding wear and to determination of toughness of ceramic/ceramic bonds. The steel envelopes are applied to predicting the angle between the fracture surface and the face of a plate.

INTRODUCTION

While research in fracture mechanics has concentrated on opening-mode loadings, a number of important instances of shear-influenced behavior are recognized. This paper discusses some examples. Attention is paid to experimental techniques, since there is no agreement as to the best means of measuring shear toughness. The resulting data are applied to several research problems, with a view towards developing a general picture of the status of mixed-mode failure envelopes and their implications for shear-related fracture phenomena.

COMBINED TENSION/LONGITUDINAL-SHEAR LOADING OF CERAMICS

Our experiments involving mixed Mode-I/Mode-II displacements were originally undertaken in order to gain insight into failure of nominally-crack-free ceramics under complex load patterns (see

* Metals and Ceramics Section, Battelle Memorial Institute, Columbus, Ohio, 43201-2693, USA

Reference (1) for a recent example of this approach). However, the work at Battelle evolved into study of two other problems: debris formation in sliding wear and shear toughness of ceramic/ceramic bonds. This section first describes our approach to evaluating mixed-mode failure envelopes of brittle materials and then presents some results that are relevant to the two problems of interest.

The Diametrally-Compressed Disk Specimen

Mixed-mode toughness of brittle materials can be measured by means of diametral compression of disks, which induces a pure tensile stress normal to the load line and a pure shear stress on a crack that is inclined at an appropriate angle. Because of this stress distribution it is possible to orient a crack to provide Mode I, Mode II, or any combination thereof. This flexibility has resulted in a number of mixed-mode failure envelopes being generated for brittle materials, e.g (2). In addition to unstable initiation, stable crack growth data in glass have been reported under shear and tensile loadings (3).

Figure 1 illustrates the test geometry. While this figure portrays a bonded specimen, the procedure is, of course, applicable to monoliths. The specimen is thin (length:diameter $\approx$ 1/10) and the notch is most easily produced by means of circular saw cuts normal to the circular faces (4). The fine microstructures of advanced ceramics insure that the notch-tip stress field will sample a representative amount of material, even when the specimen is only a few millimeters thick.

Although many mixed-mode fracture-envelopes have been proposed, we have found that the one due to Richard (5) is particularly simple and useful:

$$K_{iq}/K_{Iq} + (K_{iiq}/c_{II}K_{Iq})^2 = 1 \qquad (1)$$

where K_{Iq} is the plane-strain fracture toughness in tension, K_{iq} and K_{iiq} are the normal and shear stress intensities associated with mixed-mode fracture, and $c_{II} = K_{IIq}/K_{Iq}$ with K_{IIq} being the longitudinal-shear fracture toughness. The subscript, q, is used to emphasize that the test procedure is non-standard.

When the crack becomes unstable, it extends by kink formation and growth in an out-of-plane direction. It is possible to predict this direction of crack extension by applying the maximum-hoop-stress theory:

$$K_{iiq}/K_{iq} = \sin\phi/(3\cos\phi + 1) \qquad (2)$$

where ϕ is the angle between the original crack and the crack-extension plane.

Figure 2 shows examples of Equations (1) and (2), illustrating that these equations are suitable for modeling purposes. Note that Figure 2b was generated as an input to the wear model discussed next. In this case the specimens had straight-through notches to inhibit the crack-face rubbing that is associated with compression across the crack plane for large values of the inclination angle. Rubbing is treated independently in the model.

Modeling of Sliding Wear

As noted above, the mixed-mode experiments shown in Figures 1 and 2 were undertaken in order to aid the formulation of a linear elastic debris-formation model for sliding wear of ceramics (6). In this model, a sub-surface crack is visualized as extending under the influence of shear stresses, since the shear driving force is much larger than the normal driving force. Indeed, the normal force associated with sliding wear is compressive and hinders crack extension. While the model does not consider the criteria for formation of the sub-surface crack, it is usually assumed that ceramics contain numerous pre-existing flaws so that the controlling process in wear is likely to be crack growth and not crack formation.

The model is sketched in Figure 3. While, in reality, an asperity contact is best represented by a load distributed over a small circular contact, it is represented in the model by a line force so that a simpler plane strain calculation can be made. At the top of Figure 3 the asperity is seen to approach the subsurface crack. Both the shear and compressive stress intensities are calculated at the closer tip. With the aid of the analysis used to generate Figure 2, the crack extension direction was calculated to be at an angle of approximately 50 degrees to the free surface, so that the subsurface crack is converted into a small lip. As the asperity passes over the lip, it exerts a stress on the kink at the edge of the right-hand tip of the pre-existing crack. This stress causes a crack to extend from the kink, thus freeing the lip and creating a debris particle. It is recognized that this model must be considered speculative at this point, since experimental evidence on the debris-formation mechanism in brittle materials appears to be currently unavailable.

Extensions of the model include allowing the sub-surface crack to lie at an arbitrary direction to the free surface and varying the friction coefficients (both on the rubbing surfaces and the opposing faces of the crack). Calculations show that high sub-surface stress intensities are associated with subsurface cracks lying at a small angle to the free surface and with high free-surface friction (7).

Toughness of Ceramic/Ceramic Bonds

Majumdar, et al (8) have developed a technique for bonding mating parts of partially-stabilized zirconia using a particle-strengthened glass-ceramic interlayer. Joint efficiencies as high as 54 percent have been obtained in four-point bending (9), with failure occurring in the interlayer material. However, bend strength is not the sole criterion for joint performance, since resistance to shear forces can have a strong effect on the reliability of the joint. For this reason, the diametrally-compressed disk specimen was used to measure longitudinal-shear toughness (K_{IIq}).

Figure 4, taken from Reference (10), compares tensile and shear toughness results from Battelle on monolithic ceramics with those from the literature. A variety of designs and a number of different ceramic materials are included. Also included is a zirconia/nodular-cast-iron bond, where the crack propagated primarily in the zirconia substrate. The bonded specimens are represented by the filled point. The upper dashed line represents a 2:1 ratio ($K_{IIq} = 2\ K_{Iq}$) and the lower dashed line represents a 1:1 ratio, or $K_{IIq} = K_{Iq}$. The data divide roughly into two families. Chevron-notch diametral compression results lie closer to the higher ratio because fracture instability occurs after some stable crack growth, which induces rubbing of opposing crack faces under Mode II loading prior to instability, and which, in turn, shields the tip from the full applied shear stress intensity. This effect that has been recognized for several years (11),(12).

As a first approximation, it can be assumed that rubbing occurs when the opening-mode displacement becomes less than the amplitude of surface roughness. For example, the non-disk geometry that shows the high K_{Iq}:K_{IIq} ratio is the notched block loaded in shear, where the author noted that the fracture surfaces were so rough that interference of the relative motion of the opposing faces occurred (13).

As noted earlier, the rubbing effect can be ameliorated by using a straight-through chevron notch. However, there is a potential penalty of producing artificially high K_{Iq} values. This point was examined in Reference (6), which reported the same K_{Iq} values for both a blunt notch and a chevron crack in porcelain specimens. The Mode II data for blunt notches all lie close to the 1:1 line in Figure 4, suggesting that unscreened values of $K_{IIq} \approx K_{Iq}$.

To summarize, the results in this section suggest that K_{IIq} is on the order of K_{Iq}, provided the crack tip is not shielded by rubbing. Typically, this rubbing adds an increment of about K_{Iq} to K_{IIq}. Larger compressive loads than are used for the disk specimen will increase the crack-tip shielding and the Mode-II increment (14).

COMBINED TENSION/TRANSVERSE SHEAR LOADING OF STEEL

One objective of the experiments described in this section was to understand the conditions giving rise to either flat or slant fracture of steel plates. While flat fracture involves only Mode I displacements (in the absence of shear lips), slant fracture of plates under tension involves a mixture of Modes I and III. The discussion in this Section is directed towards analysis of the angle between the fracture plane and the planar face of the plate.

Test-specimen Design

Figure 5 illustrates the slant-notch compact specimen developed to study the Mode-I/Mode-III fracture of steel (15). Various Mode-III:Mode-I ratios are generated by varying the crack inclination angle θ, which equals $\pi/2$ in pure Mode I and assumes smaller values as a Mode III loading component is added. The compact design was chosen so that stable crack growth (R-curve behavior) could be investigated. The crack planes were stabilized by side grooves equal to 20 percent of the crack width to inhibit crack plane rotation during growth; rotation towards the specimen faces was observed in the absence of side grooves (16).

To evaluate the J-integral, displacements are measured both parallel and normal to the load line. The loads and displacements are resolved, relative to crack plane coordinates, into Mode I and Mode III components. These components are then used to determine the components J_{iq} and J_{iiiq} of the total mixed-mode value ($J_{iq} + J_{iiiq} = J_{total,q}$).

The specimen in Figure 5 is not capable of generating all possible combinations of Mode I and Mode III, since the crack plane intersects the loading holes if θ becomes too small. Accordingly, a specimen design for mode III testing was developed by Schroth, et al. (17); it is sketched in Figure 6. The specimen is placed on a flat block, which supports all of the plate except the tongue between the cracks. Loading is accomplished by pressing down on the tongue. Side grooves of 40 percent of the thickness are incorporated in order to insure that crack growth is coplanar with the starter notch.

Ratio of Mode I:Mode III Toughness

Figure 7 compares the literature data (18) with those generated cooperatively at Battelle and The Ohio State University (19), (20), (21). Similarly to Figure 4, a wide variety of steels and specimen designs is represented. Since low toughness alloys exhibit flat fracture and high toughness alloys exhibit slant fracture, it was anticipated that $J_{IIIq} > J_{Ic}$ for low-toughness steels while $J_{Ic} > J_{IIIq}$ for high toughness steels. Examination of the data compila-

tion in Figure 7 reveals that there are problems in verifying these inequalities at either end of the toughness scale. While Figure 7 shows that there is a tendency for brittle materials to lie above the 1:1 line and a slight tendency for tough materials to lie below the 1:1 line, the deviations from the line appear to be small. At the brittle end Manoharan, et al. (22) found that they could not obtain Mode III data on a brittle steel, since crack initiation was associated with crack plane rotation into a Mode I orientation, despite severe geometrical constraints. Therefore J_{IIIq} values had to be obtained by extrapolation from low θ values. On the high toughness end, visual observations of rubbing on the fracture surface give support to a shielding argument, similar to the one advanced for the Mode-I/Mode-II case discussed earlier, so that the effective J_{IIIq} is increased.

Failure Envelopes

Schroth, et al. (19) showed that the literature on high-strength alloys can be described by a fracture-toughness envelope of the form:

$$(K_{iq}/K_{Ic})^2 + (K_{iiiq}/c_{III}K_{Ic})^2 = 1 \qquad (3a)$$

It is not unexpected that Equation (3a) differs from the Mode-I/Mode-II relation (Equation 1) since, unlike Mode II, the Mode III elastic stress field is uncoupled from the Mode I stress field.

To extend the fracture envelope to tougher steels, Equation (3a) can be rewritten:

$$J_{iq}/J_{Ic} + J_{iiiq}/C_{III}J_{Ic} = 1 \qquad (3b)$$

Figure 8 illustrates the behavior of a tough steel, which gives particularly strong support to the rubbing argument. Initially, the Mode I (tensile) toughness decreases linearly with an increasing Mode III (transverse shear) component. However, as the Mode-III component increases, the curve becomes increasingly non-linear as would be expected if rubbing played a role. Curvature of the J_{iq}/J_{iiiq} plot is also seen after a small amount of stable crack growth in a second steel (19). Otherwise, the steels studied on our program obeyed Equation (3).

Another method of presenting the mixed-mode data is via the variation of fracture energy vs. initial crack angle θ (see Figure 5). Figure 9 reports the data for the same tough steel illustrated in Figure 8. There is an indication of a minimum in the curve at an angle of about 35 degrees, suggesting that this is the steady-state orientation of the fracture plane. Thus, the data in this note are consistent with the tendency for tough materials to fail by shear fracture and brittle materials to fail by tensile fracture.

COMMENTS ON THE RELATION BETWEEN RUBBING AND SHEAR TOUGHNESS

While testing and data reduction for the specimens described in this paper present no significant problems, the relation of the measured values of fracture toughness to the actual values of these quantities at the crack tip has not been resolved. The Mode-II and Mode-III shielding arising from the rubbing of the opposite faces of the crack has already been discussed. In addition, the presence of asperities on the opposing crack faces displaces the faces in a direction normal to the crack plane and gives rise to an anti-screening effect of the Mode I component of toughness, which causes its crack tip value to be greater than its nominal value (23).

The combined effects of the two mechanisms are sketched in Figure 10. The solid line in this figure represents the failure envelope generated using the techniques described in this paper. For point A, the screening caused by surface rubbing displaces the point to the left in the figure while the anti-screening associated with asperities displaces it upwards. The result is that the two effects tend to cancel one another, leading to a point A' which is the crack tip value and is closer to the nominal failure envelope than it would be if either of the effects did not operate.

The overall result of these considerations is that there are two separate failure envelopes. The nominal failure envelope (dashed line in Figure 10) is based on continuum mechanics and is a completely valid approach to defining safe operating loads and crack lengths. The crack-tip failure envelope (solid line in Figure 10) incorporates mechanistic considerations, and needs to be known in order to develop proper analyses of the effects of microstructural variables in mixed-mode fracture. Evaluating this latter envelope is a difficult problem which needs to be investigated further.

Finally, it is important to note that it is not clear that rubbing is undesirable. On the one hand, specimens free of rubbing provide actual notch-tip stress intensity values, while rubbing induces crack-tip screening and a resultant apparent elevation of stress intensity at failure. On the other hand rubbing is characteristic of the sharp crack under shear loading and thus is a real feature of crack growth. Thus, there is a dilemma in mixed-mode fracture toughness test development, which cannot be resolved at present: either use a blunt notch which can lead to non-conservative shear toughness values due to acuity effects or use a sharp crack which may lead to non-conservative toughness values due to crack-face interference. To compound the problem the minimum notch diameter to obtain the sharp-crack toughness is expected to vary with material.

CONCLUSIONS

1. Simple test procedures for measuring mixed-mode fracture toughness have been developed and applied to a variety of problems.

2. Rubbing of surfaces, associated with small opening displacements, introduces ambiguity in the measurements.

ACKNOWLEDGMENTS

The research summarized in this paper was performed as part of several programs at Battelle; the steel and ceramic-wear programs were carried out in collaboration with The Ohio State University. In addition to the colleagues cited in the Reference list, I am grateful to W. A. Glaeser, P. R. Held, A. T. Hopper, and I-H Lin (NIST). D. A. Rigney (OSU) and J. P. Hirth (Wash. St. Univ.) provided helpful comments on the manuscript.

SYMBOLS USED

C_{III} = Ratio at failure of transverse-shear-mode J-integral to opening-mode J-integral.

c_{II}, c_{III} = Ratios of shear-mode toughness to opening-mode toughness.

J_{Ic}, J_{IIIq} = Values of J-integral at failure for opening and transverse-shear, respectively, kJ/m^2.

J_{iq}, J_{iiiq} = Values at failure of components of the J-integral under mixed-mode loading, kJ/m^2.

$J_{total,q}$ = Total J-integral at failure under mixed-mode loading.

K_{Ic}, K_{Iq} = Fracture toughness, opening mode, $MPa\sqrt{m}$.

K_{IIQ} = Fracture toughness, transverse shear mode, $MPa\sqrt{m}$.

K_{iq}, K_{iiq}, K_{iiiq} = Stress intensity at failure under mixed-mode loading, $MPa\sqrt{m}$.

θ = Angle between load line and crack plane, deg.

ϕ = Angle of crack deviation at onset of growth, deg.

REFERENCES

(1) D. Singh and D. K. Shetty, Trans ASME, J. Engg. Gas Turb. Pow., vol. 111 (1989) 174-180

(2) D. Singh and D. K. Shetty, J. Amer. Ceram. Soc., vol.72 (1989) 78-84

(3) D. Singh and D. K. Shetty "Subcritical Crack Growth in Soda-Lime Glass in Combined Mode I and Mode II Loading" submitted to J. Amer. Ceram. Soc. (Feb., 1990)

(4) D. K. Shetty, A. R. Rosenfield, and W. H. Duckworth, J. Amer Ceram. Soc., vol. 68 (1985) C325-C327

(5) H.-A. Richard, pp. 423-437 in H. P. Rossamith, ed., Structural Failure: Product Liability and Technical Insurance, Interscience, Geneva (1987)

(6) A. R. Rosenfield, J. Amer. Ceram. Soc. vol. 72 (1989) 2117-2120

(7) A. R. Rosenfield: "A Model of Sliding Wear of Ceramics" submitted to J. Mater. Eng. (Sept., 1989)

(8) B. S. Majumdar, S. L. Swartz, and A. T. Hopper: "Zirconia-Zirconia Joints-Part I, Fabrication and Microstructural Characterization", submitted to J. Amer. Ceram. Soc. (April, 1990)

(9) B. S. Majumdar, J. Ahmad, and A. R. Rosenfield: "Zirconia-Zirconia Joints-Part II, Mechanical Characterization and Analysis", submitted to J. Amer. Ceram. Soc. (April, 1990)

(10) A. R. Rosenfield and B. S. Majumdar, "Fracture Toughness of Bonds using a Disk Specimen", submitted to J. Test. Eval. (May, 1990)

(11) D. B. Marshall, J. Amer. Ceram. Soc., vol. 67 (1984) 110-116

(12) J. J. Petrovic, J. Amer. Ceram. Soc., vol. 68 (1985) 348-355

(13) J. Davies, J. Mater. Sci. Let., vol. 6 (1987) 879-881

(14) S.-K. Chung, Amer. Ceram. Soc. Bull., vol. 69 (1990) 358-368

(15) M. Manoharan, J. P. Hirth, and A. R. Rosenfield, "A Suggested procedure for Combined Mode I-Mode III Fracture Toughness Testing", J. Test. Eval. (in press)

(16) M. T. Miglin, J. P. Hirth, and A. R. Rosenfield, Res Mechanica, vol. 11 (1984) 85-95

(17) J. G. Schroth, R. G. Hoagland, J. P. Hirth, and A. R. Rosenfield, Scripta Met., vol. 19 (1985) 215-219

(18) Zhou Yishu, Engg. Fracture Mech. vol.34 (1989) 891-899; J-Q. Wu, pp.2377-2386 in K. Salama, et al., eds. Advances in Fracture Research, Pergamon, Oxford (1989); M. Yoda, Engg. Fracture Mech., 26 (1987) 425-431; Z.H.Liu and W.Shen, Int. J. Fracture vol.25 (1984) R21-R29; N. Tsangarakis, Engg. Fracture Mech. vol. 19 (1984) 903-909; R. C. Shah, ASTM STP 560 (1974) 29-52;

(19) J. G. Schroth, J. P. Hirth, R. G. Hoagland, and A. R. Rosenfield, Metall. Trans. A, vol 18A (1987) 1061-1072

(20) S. Raghavachary, J. P. Hirth, and A. R. Rosenfield: "Mixed-Mode I/III Fracture Toughness of an Experimental Rotor Steel" Metall. Trans. A (in press)

(21) M. Manoharan, S. Raghavachary, J. P. Hirth, and A. R. Rosenfield, Trans ASME, J. Eng. Mater. Tech., vol. 111 (1989) 440-442

(22) M. Manoharan, J. P. Hirth, and A. R. Rosenfield, Scripta Met., vol. 23 (1989) 763-766

(23) T. S. Gross and D. A. Mendelsohn, Eng. Fract. Mech., vol. 31 (1988) 405-420

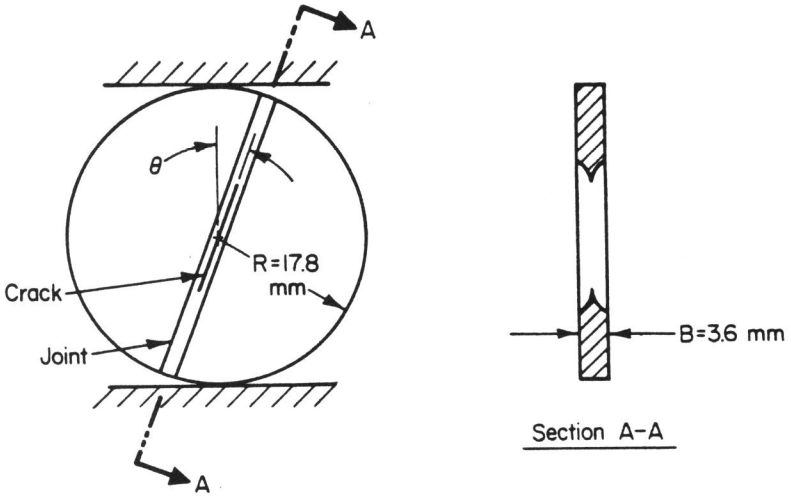

Figure 1 Chevron-Notched Cracked Disk Specimen for Measuring Mixed-Mode Fracture Toughness of Ceramic/Ceramic Joints

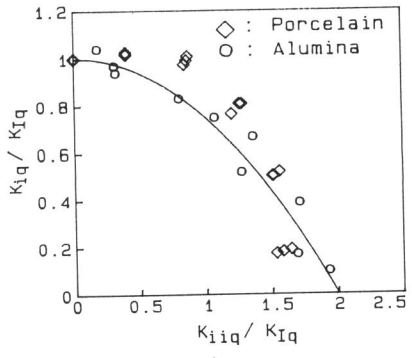

Figure 2a Fracture Toughness Envelope Obtained Using Cracked Disks

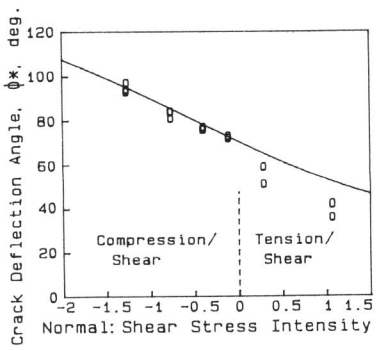

Figure 2b Effect of Shear Loads on Crack Deflection

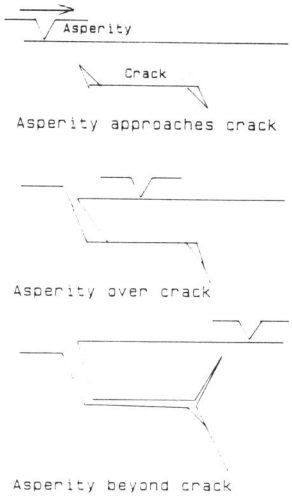

Figure 3 Preliminary Wear-Debris Formation Model for Ceramics

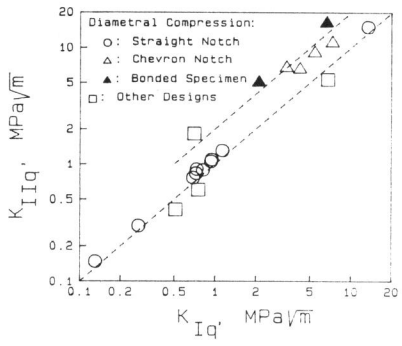

Figure 4 Opening and Longitudinal-Shear Fracture Toughness of Brittle Materials

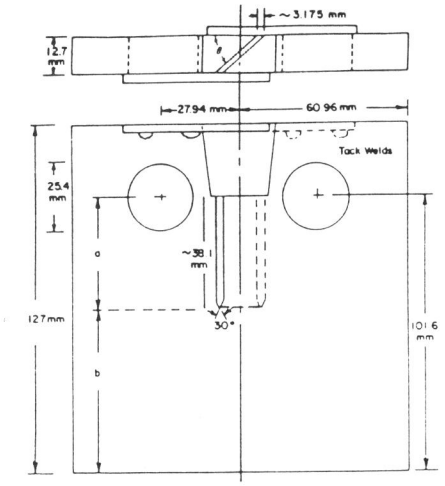

Figure 5 Modified Compact Specimen for Measuring Mixed-Mode Fracture of Steel. Side Grooves Omitted for Clarity

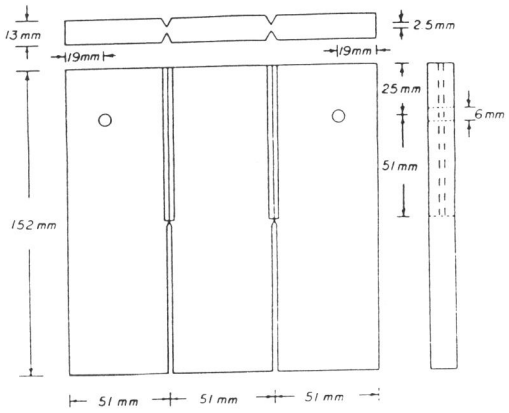

Figure 6 Mode III Test specimen for Steel.

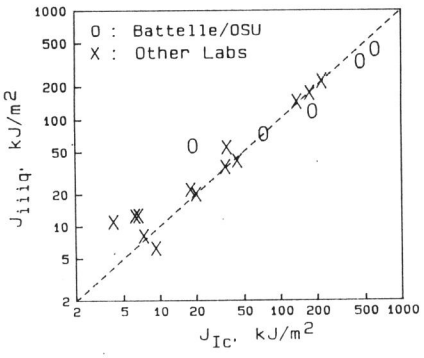

Figure 7 Comparison of J-Integral Values for Steel in Tension and Transverse Shear

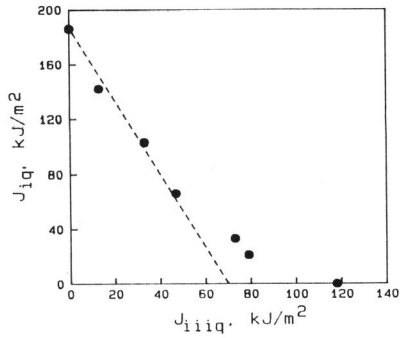

Figure 8 Mixed-Mode Failure Envelope for Ni-Cr-Mo-V Steel

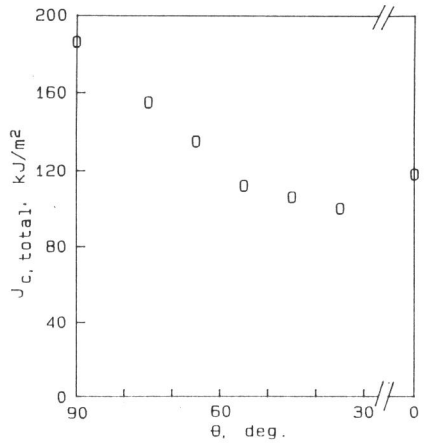

Figure 9. Effect of Crack Inclination on J-Integral for Ni-Cr-Mo-V Steel

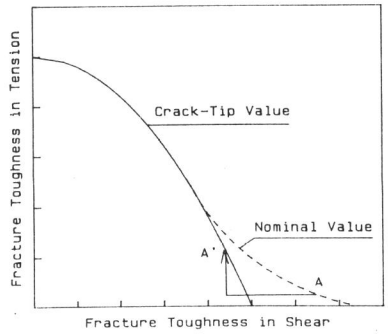

Figure 10 Effect of Surface Rubbing on Crack-Tip Screening